



## Degradation of polycrystalline rhodium and rhodium nanoparticles

Arndt Karschin<sup>a,b,\*</sup>, Ioannis Katsounaros<sup>b,1</sup>, Sebastian O. Klemm<sup>b</sup>, Josef C. Meier<sup>b,1</sup>, Karl J.J. Mayrhofer<sup>b,\*\*,1</sup>

<sup>a</sup> *Institut für Anorganische Chemie und Strukturchemie, Lehrstuhl I: Bioanorganische Chemie und Katalyse, Heinrich Heine Universität Düsseldorf, Universitätsstraße 1, 40225 Düsseldorf, Germany*

<sup>b</sup> *Abteilung für Grenzflächenchemie und Oberflächentechnik, Max-Planck-Institut für Eisenforschung, Max-Planck-Straße 1, 40237 Düsseldorf, Germany*

### ARTICLE INFO

#### Article history:

Received 28 October 2011

Received in revised form 17 March 2012

Accepted 19 March 2012

Available online 27 March 2012

#### Keywords:

Rhodium  
Noble metals  
Stability  
Dissolution  
Nanoparticles

### ABSTRACT

The electrochemical stability of polycrystalline rhodium and rhodium nanoparticles is quantitatively investigated in non-complexing sulfate electrolyte under potential cycling conditions. In situ measurements of the active surface area are complemented by discrete elemental analysis of the electrolyte solution. Rhodium electrodes are not stable and dissolve upon potential excursions into the oxide region above approximately +0.5 V<sub>RHE</sub>; the higher the positive potential limit, the higher the mass loss rate per cycle. Interestingly, the normalized catalyst mass loss is independent of the initial catalyst loading under identical conditions. The dissolution of Rh and the concomitant structural changes have to be considered in any further electrocatalytic study of this kind of electrodes.

© 2012 Elsevier Ltd. All rights reserved.

### 1. Introduction

The electrochemical properties of polycrystalline rhodium electrodes have been widely studied mostly using the cyclic voltammetry technique [1–4]. The adsorption and desorption processes of sulfate anions as well as of hydrogen and oxygen species on rhodium surfaces during potentiodynamic scans are well understood due to the aid of complementary techniques like FTIR spectroscopy [5], electrochemical impedance spectroscopy (EIS) [6,7], infrared reflection adsorption spectroscopy (IRAS) [8,9], radioactive labeling [4,10,11] or the electrochemical quartz crystal microbalance (EQCM) [12–14]. Even though rhodium as a noble metal catalyst was initially thought to be resistant to corrosion in acid electrolytes, Rand and Woods have shown that rhodium dissolution takes place during cyclic voltammetry up to sufficiently positive potentials even in non-complexing acid solutions like sulfuric acid [15]. Recently, Czerwiński and co-workers [16] as well as Juodkazis et al. [17] showed that the electrode mass

decreased during cycling, by performing EQCM measurements. Furthermore, it was shown that the rhodium dissolution is affected by the scan rate as well as by the upper potential limit [16]. The extent of dissolution from EQCM studies can then be calculated indirectly from the frequency change between consecutive cycles.

High surface area (HSA) nanocatalysts are more and more in the focus of interest due to their very high mass-normalized activities. In several reactions, rhodium alloys are used as nanoparticulate electrocatalysts as for example, Pt/Rh in ethanol oxidation [18–21] or Rh/Ir in borohydride oxidation [22]. Even though the activity of the catalytic material is typically of primary interest in many electrocatalytic studies, stability aspects are also highly important, if not more important, in particular when dealing with nanoparticulate catalysts [23–26]. Dissolution of noble metal catalyst components can severely alter the surface composition and structure and thus their electrocatalytic properties. In this paper we therefore study the stability of a polycrystalline rhodium electrode and of HSA rhodium catalysts in sulfuric acid, before investigating any electrocatalytic reaction thereon. Since the EQCM is only applicable to planar electrodes, we instead utilize a combined approach by following during electrochemical treatment both the decrease of the real (active) surface area in situ as well as the concentration of dissolved rhodium in the electrolyte by Inductively Coupled Plasma Mass Spectroscopy (ICP-MS).

\* Corresponding author at: Institut für Anorganische Chemie und Strukturchemie, Lehrstuhl I: Bioanorganische Chemie und Katalyse, Heinrich Heine Universität Düsseldorf, Universitätsstraße 1, 40225 Düsseldorf, Germany. Tel.: +49 211 6792 160; fax: +49 211 6792 218.

\*\* Corresponding author. Tel.: +49 211 6792 160; fax: +49 211 6792 218.

E-mail addresses: [akarschin@gmail.com](mailto:akarschin@gmail.com) (A. Karschin), [mayrhofer@mpie.de](mailto:mayrhofer@mpie.de) (K.J.J. Mayrhofer).

<sup>1</sup> ISE Member.

## 2. Experimental

### 2.1. Electrochemical measurements

All electrochemical experiments were carried out in a three compartment Teflon cell (see Fig. S1 in the Supporting Information) at room temperature using a Reference 600 potentiostat (Gamry, USA) and a rotating disk electrode (RDE) setup with an analytical rotation controller (Radiometer, France). A polycrystalline rhodium disk or rhodium nanoparticles (NPs) attached on a glassy carbon disk (both 0.196 cm<sup>2</sup> geometrical area and 3 mm thickness) were used as working electrodes. The polycrystalline rhodium and the glassy carbon disks were ground prior to the measurements with SiC grinding paper (2500 and 4000 grit) and polished with a 3 μm and a 1 μm diamond suspension. A graphite rod and a saturated Ag/AgCl electrode (Metrohm, Germany) placed into a Tschurl modification [27] were used as counter and reference electrodes, respectively. However, all potentials in this paper are expressed with respect to the reversible hydrogen electrode (RHE) potential. The potentiostat, the rotator and the gas flow were automatically controlled and programmed using an in-house built control software based on LabVIEW [28]. All cyclic voltammograms were recorded with a scan rate of 0.1 V s<sup>-1</sup> with a negative potential limit of always +0.07 V<sub>RHE</sub>. The experiments were performed in 0.1 M H<sub>2</sub>SO<sub>4</sub> solution under continuous Argon flow (200 mL min<sup>-1</sup>). Electrolyte solutions were freshly prepared using ultrapure water (18 MΩ, PureLabs®) and concentrated sulfuric acid (98%, Merck). All gases were of 99.999% purity (AirLiquide, France). The rotation rate of the working electrode during the degradation cycles was set to 100 rpm to ensure homogeneous mixing of dissolved rhodium species in the electrolyte. The solution resistance was compensated by positive feedback and the residual uncompensated resistance was less than 3 Ω in all experiments. Samples of the electrolyte (1 mL) were withdrawn at specific times using a syringe through a small hole in the cap of the Teflon cell (main compartment – see Supporting Information, Fig. S1). The concentration of dissolved rhodium in the samples was determined by an ICP-MS system (NexION 300X, Perkin Elmer), which was equipped with a cyclonic spray chamber and a Meinhard nebulizer operating at a pump rate of around 300 μL min<sup>-1</sup>. An internal standard (<sup>115</sup>In, 5 ppb) was added to each sample and measured parallel to <sup>103</sup>Rh to compensate for instrument fluctuations.

### 2.2. Real surface area determination

The real surface area of the Rh samples was determined based on the integration of the area of desorption of the underpotentially deposited hydrogen (so-called H<sub>UPD</sub>) during the cyclic voltammograms. For this, the saturation coverage of hydrogen on Rh (0.59 ML [29,30]) and the charge during the adsorption/desorption of a full monolayer of H<sub>UPD</sub> (221 μC cm<sup>-2</sup>) [3,30] were taken into account. The H<sub>UPD</sub> adsorption on Rh is influenced by the co-adsorption of electrolyte anions [4,8,9,11,31] and the charge integration is more prone to systematic error [32,33]; however, it is directly accessible from every degradation cycle without any interruption of the degradation experiment. Despite the fact that the exact quantitative determination may not be fully reliable, the systematic error remains constant so that this approach is sufficiently accurate to monitor relative changes in the surface area following the H<sub>UPD</sub> response.

### 2.3. Nanoparticle synthesis and film preparation

RhCl<sub>3</sub>·3H<sub>2</sub>O (10 mg, 38 μmol) and sodium(2-(diphenylphosphino)ethyl) phosphonate (11.4 mg, 38 μmol) [34] were dissolved in a 100 mL flask filled with water (30 mL)

under an Argon atmosphere. After stirring for 30 min at room temperature the solution was purged with hydrogen gas for 24 h, which resulted in a black solution of dissolved rhodium NPs. High Resolution Transmission Electron Microscopy (HR-TEM) analysis proved the existence of particles with a mean diameter of 2.2 ± 0.8 nm (see Fig. S2 in Supporting Information). The rhodium content of the prepared solution was 130 mg mL<sup>-1</sup>. In a standard procedure, 40 μL of the rhodium nanoparticle solution were pipetted on the glassy carbon disk, which corresponds to a loading of 26.6 μg<sub>Rh</sub> cm<sup>-2</sup>. The solvent was thereafter removed by vacuum evaporation in a desiccator. For higher loadings this procedure was repeated accordingly after removing the solvent from the electrode surface.

## 3. Results and discussion

### 3.1. Degradation of a polycrystalline rhodium electrode

A typical cyclic voltammogram of a polycrystalline rhodium electrode in 0.1 M H<sub>2</sub>SO<sub>4</sub> in the potential region between +0.07 V<sub>RHE</sub> and +1.07 V<sub>RHE</sub> is shown in Fig. 1A. In agreement with previous investigations in sulfuric acid electrolyte [3,16,35] the cyclic voltammogram consists of five main regions, noted in the figure: (a) hydrogen desorption (H<sub>UPD</sub> region); (b) double-layer region; (c) surface oxide formation region; (d) surface oxide reduction and (e) hydrogen adsorption (H<sub>UPD</sub> region). The cyclic voltammogram is qualitatively similar with that of a polycrystalline platinum surface [36], the only difference being the less defined double-layer region particularly in the negative scan due to the overlapping of the surface oxide reduction with the hydrogen adsorption region [10,16,37]. The oxide reduction is extending even into the H<sub>UPD</sub> region, thus the absolute currents in the negative scan are somewhat higher than in the positive scan. The response was not affected by the rotation rate, thus it was confirmed that the downward-shift of the cyclic voltammogram in the H<sub>UPD</sub> region is only due to a non-faradaic process, i.e. the superimposed oxide reduction current. The hysteresis observed between the surface oxide formation (c) and reduction (d) region is an indication of irreversible oxide formation; that is, the mechanisms of surface oxide formation and reduction are different [38]. It should be noticed that the increase of the upper potential limit shifts the oxide reduction peak toward even more negative potentials [1,35], due to more extensive irreversible oxide formation.

In order to study the degradation of a polycrystalline rhodium electrode over time, 1200 cyclic voltammograms within a fixed potential window were recorded continuously, with a scan rate of 0.1 V s<sup>-1</sup>. Thereby the concentration of dissolved rhodium in the electrolyte during the treatment was monitored by discrete sampling and elemental analysis using ICP-MS after certain amount of cycles. The lower potential limit was the same in all experiments (+0.07 V<sub>RHE</sub>) whereas three different upper potentials were used (+0.87, +1.07 and +1.27 V<sub>RHE</sub>) in the three measurements that were performed using the same procedure. The mass of rhodium *m*(Rh) in the electrolyte (in μg) was calculated by

$$m(\text{Rh}) = c(\text{Rh}) \cdot V \quad (1)$$

where *c*(Rh) is the concentration of Rh as measured by ICP-MS (in μg cm<sup>-3</sup>), and *V* is the volume of the electrolyte (in cm<sup>3</sup>) in the main compartment of the electrochemical cell. Fig. 1B shows the mass of Rh in the electrolyte vs. the number of cycles. The mass of rhodium in the electrolyte increases linearly with the number of cycles, implying a constant rate of dissolution over time. Thereby the real surface area of the polycrystalline electrode estimated from the H<sub>UPD</sub> is not changing significantly. The rate of dissolution calculated from the slope of the linear fit of the measured rhodium

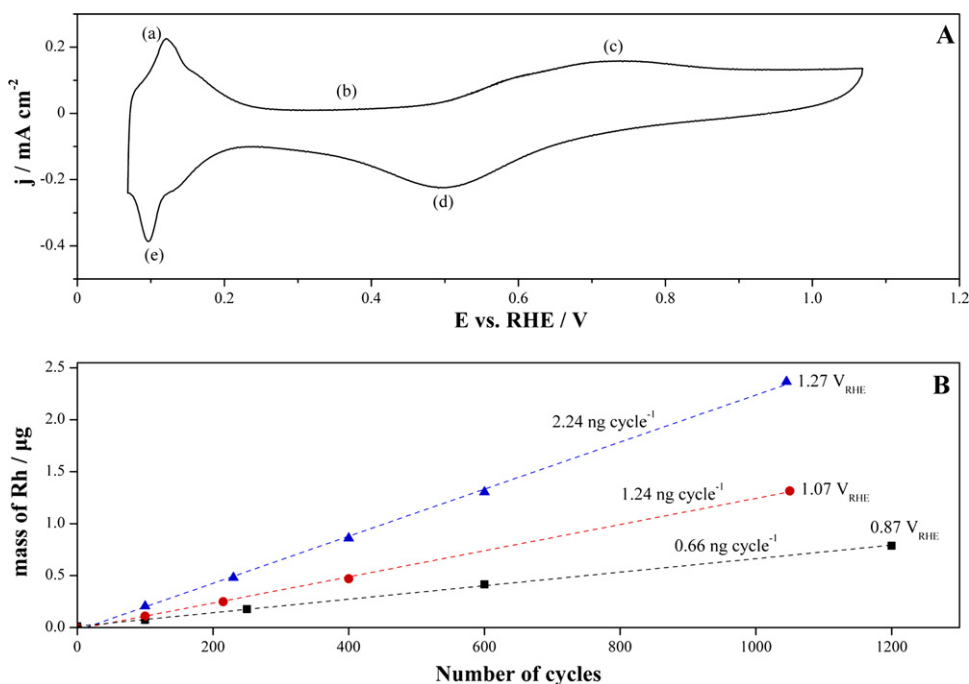


**Fig. 1.** (A) Cyclic voltammogram of a polycrystalline rhodium electrode in 0.1 M  $\text{H}_2\text{SO}_4$ . Scan rate:  $0.1 \text{ V s}^{-1}$ ; rotation rate: 100 rpm. (B) Mass of dissolved rhodium species in the electrolyte vs. the number of cycles during the degradation of a polycrystalline rhodium electrode using three different positive potential limits:  $+0.87 \text{ V}_{\text{RHE}}$  (black squares);  $+1.07 \text{ V}_{\text{RHE}}$  (red circles);  $+1.27 \text{ V}_{\text{RHE}}$  (blue triangles). The degradation rate shown in the inset corresponds to the slope of the linear fit for each experiment. (For interpretation of the references to color in this figure legend, the reader is referred to the web version of the article.)

mass increased almost linearly as the positive potential limit increases, i.e. in the order  $+0.87 \text{ V}_{\text{RHE}}$  ( $0.66 \text{ ng cycle}^{-1}$ ) <  $+1.07 \text{ V}_{\text{RHE}}$  ( $1.24 \text{ ng cycle}^{-1}$ ) <  $+1.27 \text{ V}_{\text{RHE}}$  ( $2.24 \text{ ng cycle}^{-1}$ ). This is related to the fact that the application of higher potentials causes more extensive irreversible oxide formation, as it has been shown by cyclic voltammetry for noble metals [38], which obviously increases the rate of dissolution. The exact mechanism of dissolution and the relation to the oxidation/reduction of the surface, however, is still not clear and will require further investigations. For the uppermost potential limit, taking into account the roughness factor of the electrode (1.3) the rate of  $2.24 \text{ ng cycle}^{-1}$  corresponds to a loss of  $0.04 \text{ ML cycle}^{-1}$ , which is slightly higher from that calculated from Czerwiński and co-workers under similar conditions [16].

### 3.2. Degradation of rhodium nanoparticles

In the case of nanoparticle catalysts, no rhodium features are visible during the first cycles, because the metal surface is not exposed to the electrolyte. The rhodium particles are covered by the inorganic ligand sodium(2-(diphenylphosphino)ethyl)phosphonate that is used in the synthesis procedure. Electrochemical oxidation of the ligand cleans the surface so that rhodium features start to increase gradually during the initial potential cycles and maximize after around 50–100 cycles, depending on the positive potential limit (see Fig. S3 in Supporting Information). Thus, the curve (1) in Fig. 2 shows the cyclic voltammogram of a rhodium nanoparticle catalyst (loading:  $53.2 \mu\text{g}_{\text{Rh}} \text{ cm}^{-2}$ ) after 100 cycles in the potential region between  $+0.07 \text{ V}_{\text{RHE}}$  and  $+1.07 \text{ V}_{\text{RHE}}$ . All typical rhodium features as explained above for the polycrystalline electrode (Fig. 1A regions a–e) are visible. Note, however, that the measured currents for the high surface area (HSA) catalyst are approximately one order of magnitude higher compared to that for the polycrystalline surface, due to the substantially higher roughness of the former.

When cycling the HSA catalyst for longer times, the measured currents are becoming lower and typical rhodium features are decreasing (Fig. 2), which is attributed to rhodium degradation

leading to a gradual decrease of the real surface area of the electrode. In order to study the stability of the prepared rhodium NPs, the same degradation tests as for the polycrystalline rhodium electrode were performed. In Fig. 3 the charge in the  $\text{H}_{\text{UPD}}$  region is plotted over the number of cycles, with the inset graph containing the complementary data on the mass of rhodium dissolved into the electrolyte (calculated from Eq. (1)) vs. the number of cycles, using different upper potential limits. During the first 100 cycles a very fast increase in the  $\text{H}_{\text{UPD}}$  charge is observed, which is related to the cleaning of the particles due to oxidation of the inorganic ligand. However, already at this stage a second competitive process, namely the dissolution of the particles causing a decrease of the real surface area, starts to occur in parallel and becomes dominating after full surface utilization is reached. In the case of the

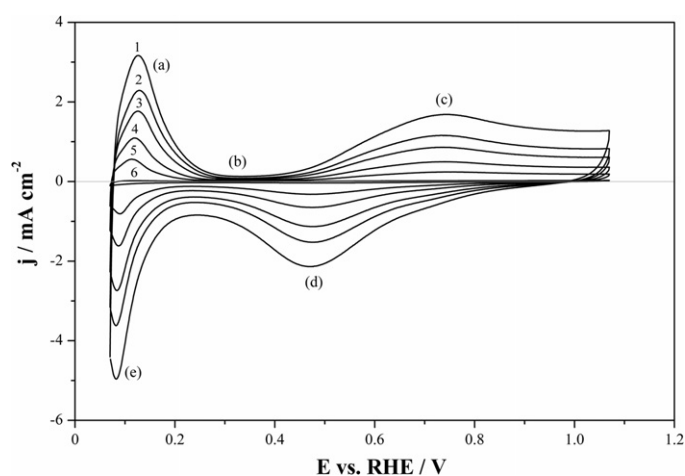


**Fig. 2.** Cyclic voltammograms of rhodium NPs ( $53.2 \mu\text{g}_{\text{Rh}} \text{ cm}^{-2}$ ) attached on glassy carbon in Ar-saturated 0.1 M  $\text{H}_2\text{SO}_4$  solution after (1) 100, (2) 175, (3) 250, (4) 375, (5) 500 and (6) 1000 cycles. Scan rate:  $0.1 \text{ V s}^{-1}$ ; rotation rate: 100 rpm.

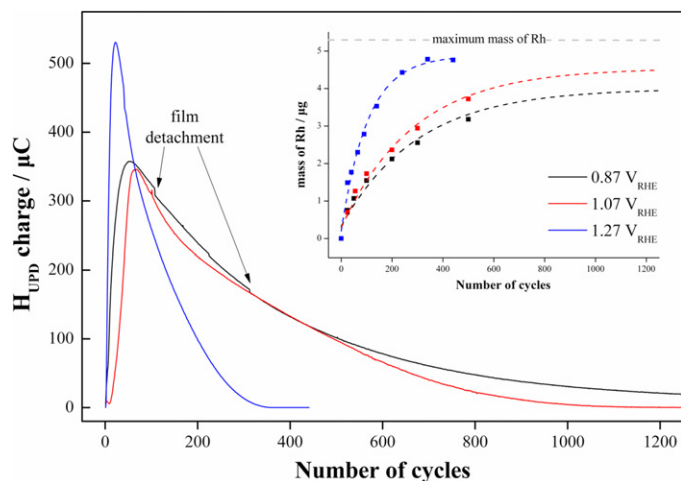


**Fig. 3.** Charge in the  $H_{UPD}$  region vs. the number of cycles during the degradation tests using different positive potential limits. The inset graph shows the measured mass of rhodium in the electrolyte vs. number of cycles, and the expected maximum mass after complete Rh dissolution ( $5.2 \mu\text{g}_{Rh}$ ). The curves in the inset serve as a guide to the eye. Rh-loading:  $26.6 \mu\text{g}_{Rh} \text{ cm}^{-2}$ ; Electrolyte:  $0.1 \text{ M H}_2\text{SO}_4$ ; scan rate:  $0.1 \text{ V s}^{-1}$ ; rotation rate:  $100 \text{ rpm}$ . Abrupt decreases of the  $H_{UPD}$  charge for  $+0.87 \text{ V}_{RHE}$  labeled with “film detachment” in the figure (not reproducible between replicates) are intentionally shown to raise the awareness for the effect of film detachment as a major technical difficulty in thin-film RDE measurements.

uppermost potential limit ( $+1.27 \text{ V}_{RHE}$ ) the highest  $H_{UPD}$  charge is obtained already after 30 cycles after a steep initial increase of the  $H_{UPD}$  charge, much earlier compared to the other upper potential limits. This implies that the increase of the upper potential limit has also a strong effect on the rate of the oxidation of the inorganic ligand, besides the accelerated dissolution of rhodium particles.

Within the two experimental data sets of  $+0.87$  and  $+1.07 \text{ V}_{RHE}$  in Fig. 3, there are some small but important differences, even though the surface area decrease seems quite similar over the first 600 cycles. In the case of an upper potential limit of  $+0.87 \text{ V}_{RHE}$  an abrupt decrease of the measured  $H_{UPD}$  charge from one CV to the next occurs, indicating catalyst film detachment from the carbon electrode. Taking this artifact into account, the true rate of mass loss is much lower for the  $+0.87 \text{ V}_{RHE}$  degradation, as can also be anticipated from the behavior beyond 600 cycles where no film detachment deteriorates the  $H_{UPD}$  decrease. Note that detachment of single particles might additionally take place. This might also be the case for the other two measurements, even though this is not visible as for the above mentioned measurement. The NPs would then precipitate on the bottom of the cell and are not sampled for the analysis, which could explain why the final mass of rhodium measured by ICP-MS is always slightly lower than the expected mass of rhodium assuming that all particles are dissolved into the electrolyte (see inset of Fig. 3). Moreover, this deviation can partially also be explained by the small amounts ( $<5\%$ ) of rhodium species detected in the reference electrode compartment due to diffusion through the Teflon hose connector. Although they are difficult to quantify, these potential systematic errors are the main determinants for the accuracy of the rate of mass loss.

In agreement with the degradation results on a polycrystalline rhodium electrode, the degradation rate on NPs again increases as the positive potential limit increases, as it can be seen by the faster decrease of the  $H_{UPD}$  charge and the faster increase of the rhodium mass for the higher potential limit experiment. For instance, in the case of an upper potential limit of  $+1.27 \text{ V}_{RHE}$ , a complete degradation of the nanoparticle catalyst occurs already after 400 cycles, whereas in the case of an upper potential limit of  $+0.87 \text{ V}_{RHE}$  the degradation process takes more than 1000 cycles. The increase of the mass of rhodium in the electrolyte does not increase linearly

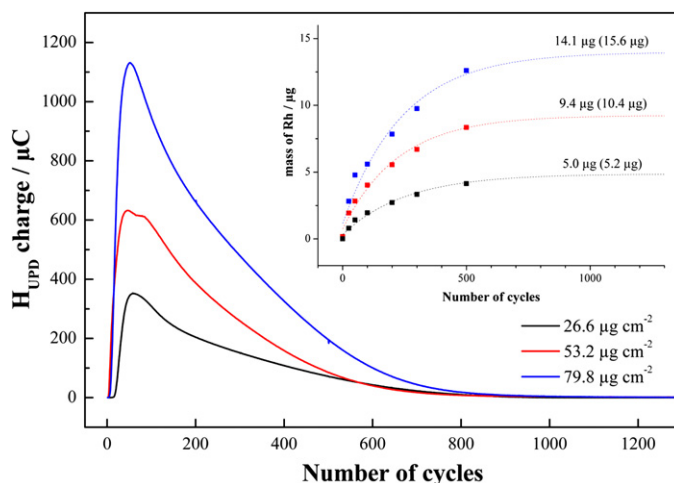


**Fig. 4.** Charge in the  $H_{UPD}$  region vs. number of cycles using different catalyst loadings. The inset graph shows the mass of rhodium in the electrolyte measured with ICP-MS vs. the number of cycles. For each measurement, the final measured mass of rhodium is given, as well as the expected mass (in brackets) if the entire catalyst was dissolving. The upper potential limit was  $+1.07 \text{ V}$  in all measurements.

with the number of cycles, as for the bulk electrode (Fig. 1A) because the real surface area of the electrode (i.e. the surface roughness) decreases during the treatment.

In order to investigate further the influence of the surface roughness on the rate of mass loss, additional degradation experiments were performed within a potential window of  $+0.07$  and  $+1.07 \text{ V}_{RHE}$  using different catalyst loadings of the rhodium NPs. As it is shown in Fig. 4 the charge in the  $H_{UPD}$  region and the mass of rhodium in the electrolyte (calculated from Eq. (1)) both depend on the loading as well. Note that again the measured final mass of rhodium in the electrolyte is always slightly (5–10%) lower than the expected one (see value in brackets in the inset), if we assume that no catalyst is remaining on the glassy carbon after the treatment. Regardless of the loading, the catalyst was fully degraded after about 1000 cycles, in line with the measurement shown in Fig. 3 for the same potential window.

When the measured mass of rhodium in the electrolyte was normalized to the corresponding mass of rhodium that was initially deposited on the glassy carbon substrate for all three loadings, then the percentage of the rhodium that was dissolved vs. the number of cycles was the same, regardless of the loading (see Fig. 5). The same is also true for the loss of rhodium surface area normalized to the area after 60 cleaning cycles (see inset in Fig. 5). This proves that the rate of catalyst mass loss is directly proportional to the Rh surface in contact with electrolyte, and explains the profile of the dissolved mass vs. number of cycles for the case of NPs. In addition, it shows that a single degradation rate cannot be deduced for the nanoparticles from these data, since it continuously changes over time.

The investigations of the stability of this kind of NP electrodes now set the basis for upcoming electrocatalytic investigations. It is clear that under the conditions presented in this manuscript, the cluster network undergoes severe morphological changes and that different approaches have to be employed accordingly in order to retrieve reproducible and meaningful data on activity. Further studies will also try to reveal the microscopic structure that develops during the potential cycling treatment, which is not clear at the moment but will additionally help to understand the NP electrode degradation. Most importantly, utilizing our novel direct coupling of an electrochemical flow cell to the ICP-MS we will try to shed more light onto the exact dissolution mechanism of Rh electrodes

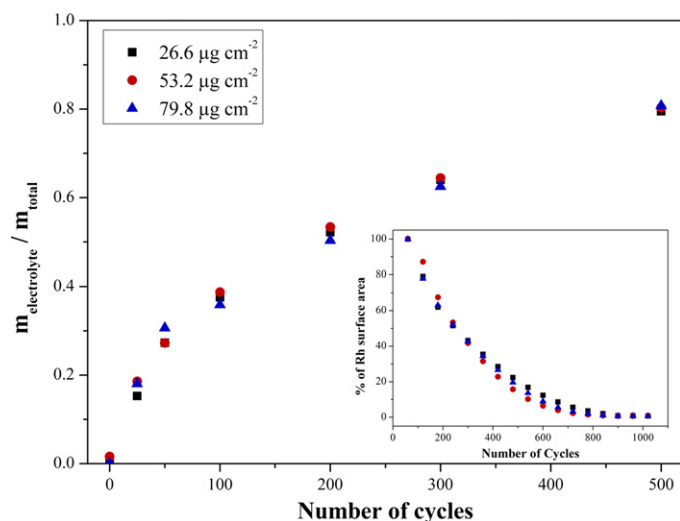


**Fig. 5.** Mass of rhodium in the electrolyte as measured by ICP-MS (data used from the inset of Fig. 4) for different loadings, normalized to the total mass of rhodium deposited on the glassy carbon, respectively. The inset shows the % Rh surface area where the normalization was done to the area after 60 cleaning cycles; data used from Fig. 4 after every 60 cycles are presented. The upper potential limit was +1.07 V in all measurements.

[39] by on-line monitoring of the dissolution of rhodium under both potentiostatic and potentiodynamic conditions.

#### 4. Conclusions

Rhodium catalysts on glassy carbon electrodes are not stable during potentiodynamic scans in non-complexing 0.1 M H<sub>2</sub>SO<sub>4</sub> within the examined potential window of +0.07 to +0.87 V<sub>RHE</sub>, and dissolve into the electrolyte during continuous cycling. The mass loss is dependent on the extent of surface oxide formation and therefore amplified by increasing the upper potential window up to +1.27 V<sub>RHE</sub> for both the polycrystalline rhodium and the rhodium nanoparticles. It was found that the rate of mass loss is proportional to the real surface area of rhodium nanoparticles, or in other words, that the rate of mass loss scales with the loading of the nanoparticles. Due to the fact that the real surface area of nanoparticles changes during cycling, a straightforward calculation of mass loss rates from the presented data for the nanoparticulate catalysts is not feasible.

#### Acknowledgements

We thank Andrea Mingers for the measurement of all ICP-MS data. J.C.M. acknowledges financial support by the Kekulé Fellowship from the Fonds der Chemischen Industrie (FCI).

#### Appendix A. Supplementary data

Supplementary data associated with this article can be found, in the online version, at doi:10.1016/j.electacta.2012.03.079.

#### References

- [1] C. Pallotta, N.R. de Tacconi, A.J. Arvia, *Electrochim. Acta* 26 (1981) 261.
- [2] F. Villiard, G. Jerkiewicz, *Can. J. Chem.* 75 (1997) 1656.
- [3] G. Jerkiewicz, J.J. Borodzinski, *Langmuir* 9 (1993) 2202.
- [4] P. Zelenay, G. Horányi, C.K. Rhee, A. Wieckowski, *J. Electroanal. Chem.* 300 (1991) 499.
- [5] I.R. de Moraes, F.C. Nart, *J. Brazil. Chem. Soc.* 12 (2001) 138.
- [6] V. Horvat-Radošević, K. Kvastek, *J. Electroanal. Chem.* 566 (2004) 451.
- [7] B. Łosiewicz, R. Jurczakowski, A. Lasia, *Electrochim. Acta* 56 (2011) 5746.
- [8] Y. Shingaya, M. Ito, *J. Electroanal. Chem.* 372 (1994) 283.
- [9] Y. Shingaya, M. Ito, *J. Electroanal. Chem.* 467 (1999) 299.
- [10] M. Wasberg, G. Horányi, *J. Electroanal. Chem.* 386 (1995) 213.
- [11] G. Horányi, M. Wasberg, *J. Electroanal. Chem.* 404 (1996) 291.
- [12] M. Wasberg, J. Bácskai, G. Inzelt, G. Horányi, *J. Electroanal. Chem.* 418 (1996) 195.
- [13] L. Salgado, G. Trejo, Y. Meas, T. Zayas, *J. Solid State Electrochem.* 10 (2006) 230.
- [14] R.T.S. Oliveira, M.C. Santos, L.O.S. Bulhões, E.C. Pereira, *J. Electroanal. Chem.* 569 (2004) 233.
- [15] D.A.J. Rand, R. Woods, *J. Electroanal. Chem.* 35 (1972) 209.
- [16] M. Łukaszewski, H. Siwek, A. Czerwiński, *Electrochim. Acta* 52 (2007) 4560.
- [17] K. Juodkasis, G. Stalnonis, B. Šebeka, V. Šukienė, I. Savickaja, *Russ. J. Electrochem.* 38 (2002) 1157.
- [18] F.H.B. Lima, E.R. Gonzalez, *Electrochim. Acta* 53 (2008) 2963.
- [19] K. Bergamaski, E.R. Gonzalez, F.C. Nart, *Electrochim. Acta* 53 (2008) 4396.
- [20] J.P.I. de Souza, S.L. Queiroz, K. Bergamaski, E.R. Gonzalez, F.C. Nart, *J. Phys. Chem. B* 106 (2002) 9825.
- [21] A. Kowal, M. Li, M. Shao, K. Sasaki, M.B. Vukmirovic, J. Zhang, N.S. Marinkovic, P. Liu, A.I. Frenkel, R.R. Adzic, *Nat. Mater.* 8 (2009) 325.
- [22] V. Kiran, T. Ravikumar, N.T. Kalyanasundaram, S. Krishnamurthy, A.K. Shukla, S. Sampath, *J. Electrochem. Soc.* 157 (2010) B1201.
- [23] Y. Shao-Horn, W. Sheng, S. Chen, P. Ferreira, E. Holby, D. Morgan, *Top. Catal.* 46 (2007) 285.
- [24] J.K. Nørskov, T. Bligaard, J. Rossmeisl, C.H. Christensen, *Nat. Chem.* 1 (2009) 37.
- [25] K.J.J. Mayrhofer, M. Arenz, *Nat. Chem.* 1 (2009) 518.
- [26] K.J.J. Mayrhofer, J.C. Meier, S.J. Ashton, G.K.H. Wiberg, F. Kraus, M. Hanzlik, M. Arenz, *Electrochem. Commun.* 10 (2008) 1144.
- [27] K.J.J. Mayrhofer, S.J. Ashton, J. Kreuzer, M. Arenz, *Int. J. Electrochem. Sci.* 4 (2009) 1.
- [28] A.A. Topalov, I. Katsounaros, J.C. Meier, S.O. Klemm, K.J.J. Mayrhofer, *Rev. Sci. Instrum.* 82 (2011) 114103.
- [29] R. Woods, *J. Electroanal. Chem.* 49 (1974) 217.
- [30] D.A.J. Rand, R. Woods, *J. Electroanal. Chem.* 31 (1971) 29.
- [31] O.A. Petrii, A.N. Frumkin, Yu G. Kotlov, *Sov. Electrochem.* 5 (1969) 686.
- [32] K.J.J. Mayrhofer, D. Strmcnik, B.B. Blizanac, V. Stamenkovic, M. Arenz, N.M. Markovic, *Electrochim. Acta* 53 (2008) 3181.
- [33] T.J. Schmidt, H.A. Gasteiger, G.D. Stab, P.M. Urban, D.M. Kolb, R.J. Behm, *J. Electrochem. Soc.* 145 (1998) 2354.
- [34] J. Glöckler, S. Klützke, W. Meyer-Zaika, A. Reller, F.J. Garcia-Garcia, H.H. Strehlow, P. Keller, E. Rentschler, W. Kläui, *Angew. Chem. Int. Ed.* 46 (2007) 1164.
- [35] M. Vukovic, *J. Electroanal. Chem.* 242 (1988) 97.
- [36] K. Ohashi, K. Sasaki, S. Nagaura, *Bull. Chem. Soc. Jpn.* 39 (1966) 2066.
- [37] N.D. Sverdlova, W. Schäfer, G.N. Mansurov, O.A. Petrii, *Russ. J. Electrochem.* 31 (1995) 227.
- [38] P. Stonehart, H.A. Kozłowska, B.E. Conway, *Proc. R. Soc. Lond. A* 310 (1969) 541.
- [39] S.O. Klemm, A.A. Topalov, C. Laska, K.J.J. Mayrhofer, *Electrochem. Commun.* 13 (2011) 1533.